An Explicit Method for Simulation of Quasi-brittle Materials and Structures Based on Peridynamic Theory

H. David Miranda / Chris Williams / John Orr

Dep. Architecture and Civil Eng. University of Bath
Claverton Down, Bath, North East
Somerset BA2 7AY, UK

Despite the massive use of concrete by the construction industry, its optimisation remains a scientific and engineering challenge that has important implications for the global environment and economy. Difficulties predicting the material behaviour after cracking are part of the problem, since design relies on accurate models. As the cracks start to grow, the hypothesis of material continuity that is critical to the differential equations of the classical theory becomes obsolete. In fact, many issues are documented in the literature regarding the employment of the classical continuum solid mechanics and the finite element method in this context. In order to avoid these problems, the recent peridynamics theory [1] was formulated without differential equations or continuity requirement.

This contribution describes a numerical method to solve the peridynamics equations using a simple explicit scheme based on the Euler method [2], where the spatial discretisation consists of a finite set of material particles and interparticle bonds. Cracks may develop by disruption of these interparticle bonds. The onset and evolution of discrete cracks in tensile zones is predicted in this paper using simple examples. The formulation of the method, comparison with the elastic theory and derivation of relations between model parameters and macroscopic elastic modulus are presented. Furthermore, an initial investigation of the model's ability to reproduce damage through the spontaneous formation of cracks during loading is analysed. The obtained results may improve the models used to describe quasi-brittle materials vulnerable to cracking and concrete structures in particular. Those improved models may lead to developments in research and application of brittle materials, higher construction quality in civil engineering and mitigation of environmental issues.

Keywords: Peridynamic, Particle systems, Fracture, Quasi-brittle, Explicit methods

1 Introduction

In terms of material modelling, relatively high success has been achieved using the standard continuum mechanics framework to predict the behaviour of certain classes of materials such as rubbers and metal alloys. However, it is generally accepted that equivalent predictive capacity has not yet been achieved using continuum damage mechanics, despite the endeavour of the scientific community.
When the cracks become large enough, the hypothesis of material continuity becomes inappropriate. In fact, the derivatives from the differential equations of continuum solid mechanics do not exist at points of discontinuity. The consequences from that assumption become apparent when employing frameworks like the Finite Element Method(FEM). To avoid the aforementioned issue, the Peridynamic theory [1][3] was developed. This theory considers an integral formulation, which remains valid despite any disruptions of the material continuity that may occur, since no space derivatives are employed. Inspired by those mentioned contributions, this work describes a numerical method to solve the peridynamics equations, using an explicit scheme, where the spatial discretisation consists in a finite set of material particles and inter-particle bonds.
This text is organized as follows: Firstly, the mathematical principles behind the method are reviewed in section 2. Secondly, the interaction function behind the proposed model is described in section 3. The numerical scheme is detailed in sections 4 and 5. Validation examples are described in section 6. Section 7 discusses possible conditions of stability for the algorithm. Section 8 describes how to relate the algorithm parameters with the elasticity of the bulk material. The simulation of the brittle behaviour of a beam is reported in section 9. Finally, the main conclusions of this work are synthesised and future works are proposed in the final section.

2 Mathematical Formulation

As previously mentioned, the theoretical framework of fundamental equations is described in the peridynamics theory proposed by Silling [1] and detailed in other articles (see for instance [4][5][6]). The peridynamic framework does not require permanent continuity of the domain, since it uses a integral formulation, in contrast to classical continuum mechanics. This property is very convenient since the continuity of the domain can be disrupted with the development of cracks. In the following a general overview of this theory is provided (refer to [1], for a more detailed description).
The peridynamic theory relies on the main assumption that the bodies are constituted by an infinite set of material particles interacting with each other through pairwise forces, in analogy to what occurs in molecular dynamic models. However, interactions only occur between pairs of particles closer than a certain maximum distance. The interaction force that each pair of particles $(1,2)$ develop per unit of volume in the Eularian configuration $\mathbf{f}_{12}$ is a function of their initial positions $\mathbf{X}_1$, $\mathbf{X}_2$ and their displacements $\mathbf{u}_1$, $\mathbf{u}_2$ according to Eq.(1).

$$\mathbf{f_{12}} = \mathbf{f_{12}}(\mathbf{u_2} - \mathbf{u_1}, \mathbf{X_2} - \mathbf{X_1}) \tag{1}$$

A more compact form for Eq.(1) is described in terms of relative positions $\Delta\mathbf{X} = \mathbf{X_2} - \mathbf{X_1}$ and relative displacements $\Delta\mathbf{u} = \mathbf{u_2} - \mathbf{u_1}$ according to Eq.(2).

$$\mathbf{f}_{12} = \mathbf{f}_{12}(\Delta\mathbf{u}, \Delta\mathbf{X}) \tag{2}$$

This interaction between the generic particles located at , $\mathbf{X_1}$ and $\mathbf{X_2}$ among other particles is represented in Fig. 1.

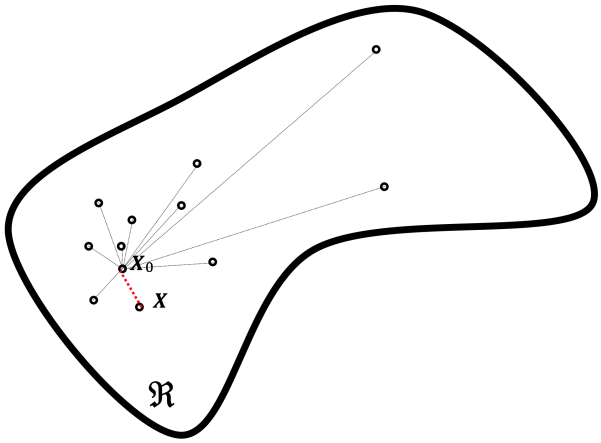

Figure 1: Possible interactions between the particle at X_1 and other particles of the body, the interaction with the particle at X_2 is highlighted [7].

From the previous statements it follows that, the resultant of all the interactions per unit of volume $\mathbf{l}(\mathbf{X})$ acting on a generic particle at the initial position $\mathbf{X}$, can be obtained by integration under the domain of the body $\mathscr{R}$, as given by Eq.(3).

$$\mathbf{l}(\mathbf{X}) = \int_{\mathscr{R}} \mathbf{f}_{12}(\mathbf{u}_0 - \mathbf{u}, \mathbf{X}_0 - \mathbf{X}) d\mathbf{X}_0 \tag{3}$$

If a generic point located at coordinates $\mathbf{X}$, with mass per unit volume ρ , and acceleration $\ddot{\mathbf{u}} = \ddot{\mathbf{u}}(\mathbf{X})$ is actuated through its volume by body forces $\mathbf{b} = \mathbf{b}(\mathbf{X})$, then the peridynamic equation of motion [1] is described by Eq.(4).

$$\rho\ddot{\mathbf{u}} = \mathbf{l} + \mathbf{b} \tag{4}$$

In particular, the static equilibrium with no body forces actuating, is defined in Eq.(5).

$$\mathbf{l} = \mathbf{0} \tag{5}$$

3 Model description

The constitutive model is defined by the interaction function. For this particular model the interaction function is given in the following Eq.(6).

$$\mathbf{f}_{12}(\Delta\mathbf{u},\Delta\mathbf{X},\alpha) = \alpha\,\frac{K}{|\Delta\mathbf{X}|}\tilde{\varepsilon}_{12}\,(\Delta\mathbf{u}+\Delta\mathbf{X}) \tag{6}$$

In Eq. (6), K is a scalar material parameter representing the the connections stiffness while $\tilde{\varepsilon}_{12}$ is a strain measure defined according to Eq.(7).

$$\tilde{\varepsilon}_{12}(\Delta\mathbf{u},\Delta\mathbf{X}) = \frac{(\Delta\mathbf{X}+\Delta\mathbf{u})^2 - \Delta\mathbf{X}^2}{2\Delta\mathbf{X}^2} \tag{7}$$

The state variable α , is employed to indicate the possibility of the interaction to be disrupted and is given by Eq.(8).

$$\alpha = \begin{cases} 1 & \text{if } \kappa_{12} \leq \tilde{\varepsilon}_{crack} \\ 0 & \text{otherwise} \end{cases} \tag{8}$$

In the previous equation κ_{12} indicates the maximum value achieved by $\tilde{\varepsilon}_{12}$, according to Eq.(9).

$$\kappa_{12} = \max\{\tilde{\varepsilon}_{12}\} \tag{9}$$

Notice that to compute $\tilde{\varepsilon}_{12}$ using Eq.(7), no square roots are requiered resulting in efficiency gains. See [8] for more details.

4 Particle dynamics algorithm

To solve the the peridynamic problem stated above, an explicit scheme was employed. Using this scheme Newton's second law is integrated for each particle in order to obtain their positions. According Newton's second law the acceleration $\ddot{\mathbf{x}}$ is given by Eq.(10)[9].

$$\ddot{\mathbf{x}} = \frac{1}{m}\left(\mathbf{F}^{\mathbf{int}} + \mathbf{F}^{\mathbf{ext}}\right) \tag{10}$$

The scalar m represents the mass of the particle, while the vectors $\mathbf{F}^{\mathbf{int}}$ and $\mathbf{F}^{\mathbf{ext}}$ represent respectively the internal forces, and external forces. The internal forces are the ones obtained by interaction with other particles of the body and given by Eq.(6). The external forces are the ones externally applied, e.g. self weight or external loading. Considering $\mathbf{F}^{\mathbf{int}}$ and $\mathbf{F}^{\mathbf{ext}}$ constant during a small time step Δt , the velocity $\dot{\mathbf{x}}$ can be approximated by Eq.(11) [9].

$$\dot{\mathbf{x}}(t_i+\Delta t) \approx \frac{1}{m}\left(\mathbf{F}^{\mathbf{int}} + \mathbf{F}^{\mathbf{ext}}\right)\Delta t + \dot{\mathbf{x}}(t_i) \tag{11}$$

Here t_i and $t_i+\Delta t$, represent two instants of time separated by a small time step. If the velocity can be considered during the small time step then the position $\mathbf{x}$ can be approximated by Eq.(12) [9].

$$\mathbf{x}(t_i+\Delta t) \approx \frac{1}{m}\dot{\mathbf{x}}(t_i+\Delta t)\Delta t + \mathbf{x}(t_i+\Delta t) \tag{12}$$

5 Description of the Algorithm

The system is composed by a set of M material particles, and a set of N fibres connection pairs of particles. Each particle $j \in [1,\ldots,M]$ consists of:

- position $\mathbf{x_j}$
- velocity $\mathbf{v_j}$

- resultant interaction force $\mathbf{f_j}$
- externally applied force $\mathbf{f_j^{ext}}$
- logical flags indicating the particle constrains $\mathbf{c_j}$
- particle constrain's velocity $\mathbf{v_{jc}}$
- mass m_j

Each fibre $i \in [1,\ldots,N]$ connects two particles 1 and 2 consists of:

- logic flag indicating if the fibre is broken α_i
- the numbers of particles that connects 1 and 2
- material reference

After the initialization of the material particles and the fibres. The algorithm loop over the time t, with increments Δt, considering the following instructions:

1: **for** each time step **do**
2: $t = t + \Delta t$
3: **for** each fibre i (connecting particles 1 and 2) **do**
4: update broken flag: $b_i = b(\mathbf{x_1}, \mathbf{x_2})$
5: compute interaction force: $\mathbf{f_i} = \mathbf{f}(\mathbf{x_1}, \mathbf{x_2}, \alpha_\mathbf{i})$
6: sum the interaction force to the particles: $\mathbf{f_1} = \mathbf{f_1} + \mathbf{f_i} \quad \mathbf{f_1} = \mathbf{f_2} - \mathbf{f_i}$
7: **end for**
8: **for** each particle j **do**
9: sum the external loads to the particles: $\mathbf{f_j} = \mathbf{f_j} + \mathbf{f_j^{ext}}$
10: update velocity: $\mathbf{v_j} = \mathbf{v_j} + \Delta t\, \mathbf{f_j}/m_j$
11: **if** j is constrained $(\mathbf{c_j} \neq \mathbf{0})$ **then**
12: set velocity to match the constrain: $\mathbf{v_j} = \mathbf{v_{jc}}$
13: **end if**
14: update position: $\mathbf{x_j} = \mathbf{x_j} + \mathbf{v_j}\Delta t$
15: reset the interaction force: $\mathbf{f_j} = \mathbf{0}$
16: **end for**
17: **end for**

.

Each time increment corresponds to a calculation cycle, where the particle's positions and other physical quantities are updated following Eq.(6) to Eq.(12). The broken fibre flag update in line (4) is described by Eqs.(7) to (9). Therefore, if a threshold elongation is achieved the fibre breaks. The computation of the interaction force on line (5) is given as a function of the elongation between the connected particles, according to the Eq.(6) and Eq.(7), and it is set to zero if the fibre is broken as previously mentioned.
The was implemented in the C programing language and for post processing of the results, software Paraview[10] and Matlab[11] were employed.

6 Comparisons with FEM and the classical elastic theory

Linear elements

A clamped beam and a Cantilever beam, subjected to a load $p = 10kN/m$, with the geometry and boundary conditions and loadings schematised in Fig.2 were considered.

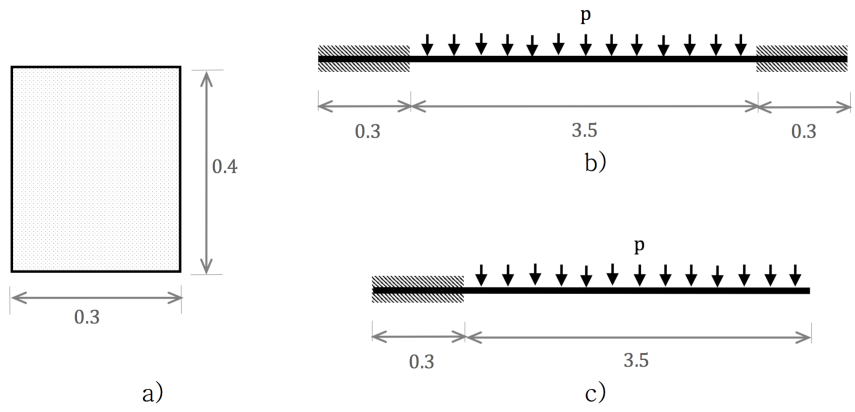

Figure 2: Geometry and boundary conditions of two beams: a) cross section; b) clamped beam; c) Cantilever beam.

Tab.1, indicates the loading and material parameters considered.

Table 1: Material parameters of the beams.

E	ν
20GPa	0.25

The particle model considered for the clamped beam is represented in Fig.3.

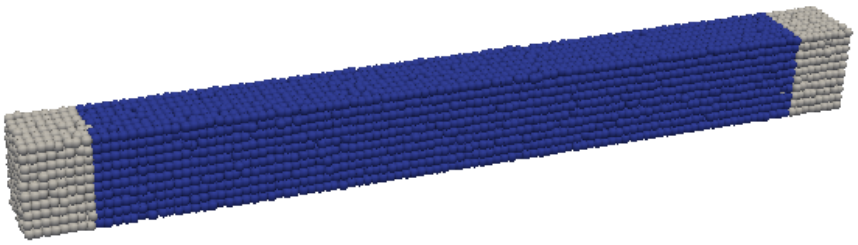

Figure 3: Numerical model considered for the clamped beam. The white nodes are constrained to move, while the nodes on blue are free to move.

In Fig.4 and Fig.5 is represented the deflection divided by the maximum deflection δ_y/δ_y^{max}, obtained for the particle model in comparison with the analytical formulation prediction for both of the beams.
The maximum deviation of the particle algorithm to the analytical prediction, was smaller than 6% for the clamped beam, and 2% for the Cantilever beam. The parameters considered for the beams are indicated in Tab.2 and Tab.3.
Forty minutes were required to compute each of the numerical models using a single processor core in a laptop computer with a 2.5GHz Intel Core i7 processor and 16GB of operating memory.

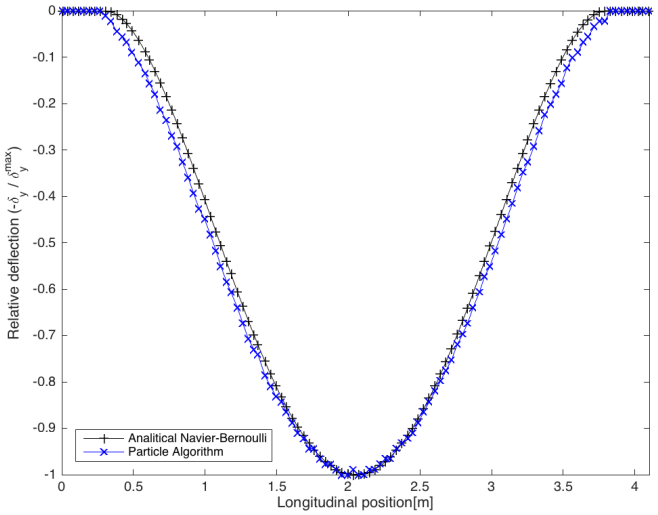

Figure 4: Comparison of deflections for the clamped beam.

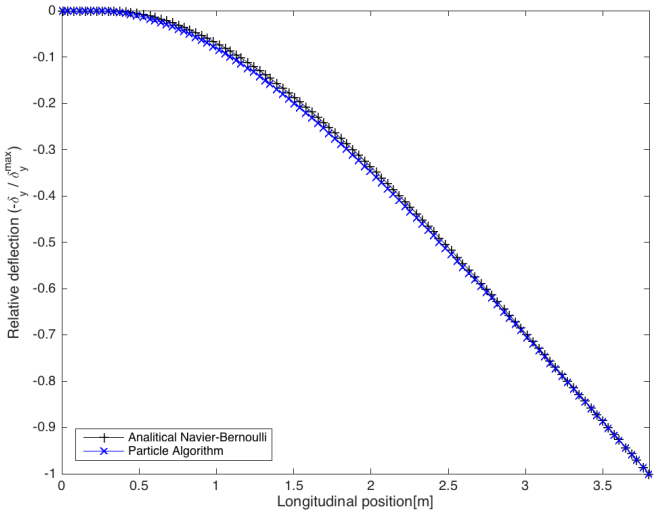

Figure 5: Comparison of deflections for the Cantilever beam.

Table 2: Parameters of the particle model for the clamped beam.

Total time	60s	Time step	0.5e-3s
No. particles	7 560	No. fibers	1 337 637
Density	1.475e3kg/m3	Mass scale factor	1000

Table 3: Parameters of the particle model for the Cantilever beam.

Total time	60s	Time step	0.5e-3s
No. particles	8 160	No. fibers	1 468 483
Density	1.718e3kg/m3	Mass scale factor	1000

Plate with three edges built in

The rectangular plate with material properties indicated in Tab.1 and represented in Fig.6, with three edges built in and the fourth edge free, subjected to a uniformly distributed load

$p = 10$kN/m was considered.

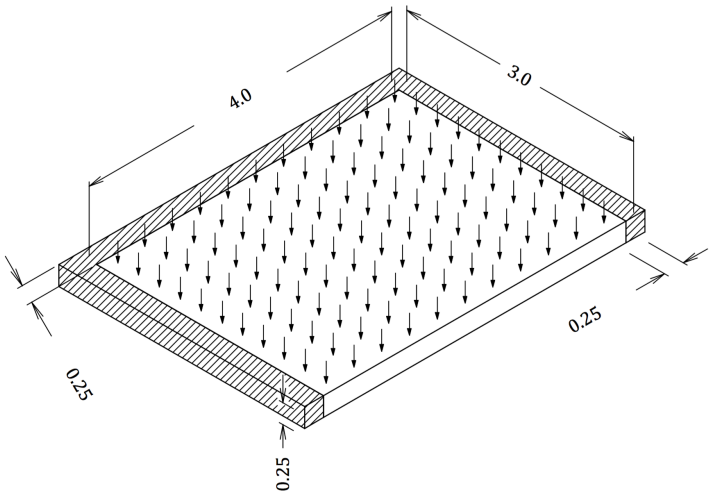

Figure 6: Model of a rectangular plate, the hatched zones are completely constrained (dimensions in meters).

The deflection field obtained $\delta_z(x,y)$ using the FEM and the proposed algorithm are presented in Fig.7.

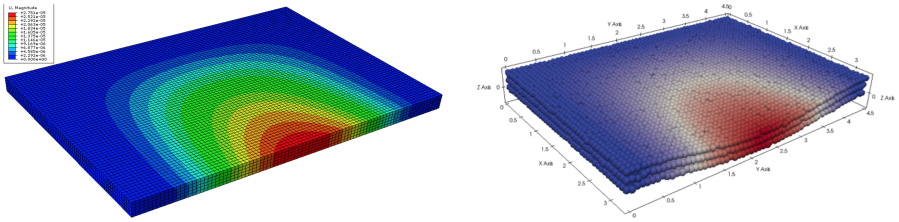

Figure 7: Contour plot of the deflection, obtained using: the FEM[12] on left and the proposed method on right.

The results from both of the methods were compared in terms of deflection divided by maximum deflection δ_z/δ_z^{max}. The results for that comparison along two perpendicular directions are represented in Fig.8 and Fig.9.

The maximum deviation between predictions is 5.5% along the free edge and 2.5% in the central line perpendicular to the free edge. The parameters considered for the particle model of the plate are indicated in Tab.4. The computational time required for the simulation of the plate was 46 minutes.

Table 4: Parameters of the particle model for the plate simulation.

Total time	60s	Time step	0.5e-3s
No. particles	7 740	No. fibers	1 259 951
Density	203.2kg/m3	Mass scale factor	1000

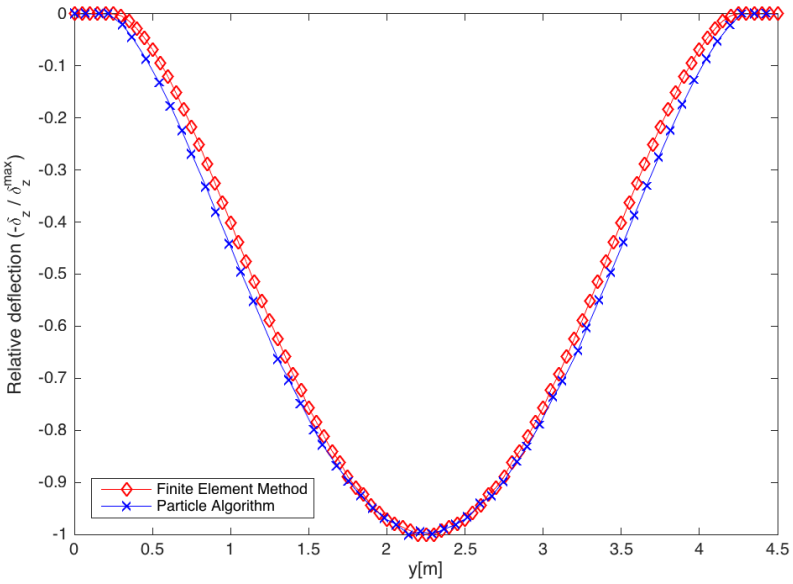

Figure 8: Plate deflection divided by maximum deflection, along the free edge.

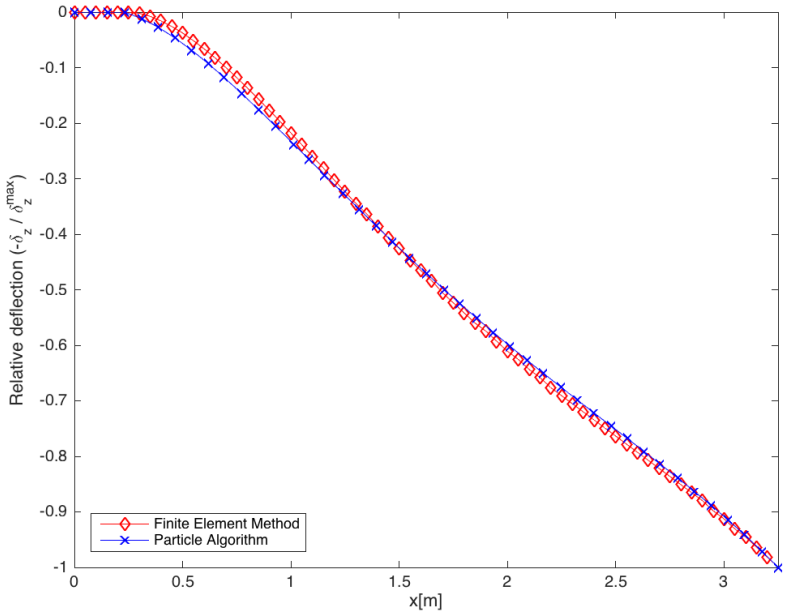

Figure 9: Plate deflection divided by maximum deflection, along the central line perpendicular to the unconstrained edge.

7 Stability

The computation time required for the simulation becomes an important problem while addressing realistic problems with complex geometry and a large amount of particles. To reduce the computation time it is important to divide the time into as few steps as possible, which increases the length of each step. Although large time steps reduce the computation time, they also lead to instability in the particle system. If the system becomes unstable, it may diverge and

degenerate in to unphysical configurations. For instance, the system can explode with particles traveling at very high speeds and quickly reaching to positions far beyond the limits of the numerical representation.

Despite no exact expression existing for the maximum stable time step Δt_{cr} , some expressions can provide an initial approximation. One of those expressions is the classical Courant–Friedrichs–Lewy condition[13], Eq.(13), developed to study the convergence of the finite differences method while addressing certain deferential equations.

$$\Delta t_{cr} \sum_i \frac{u_i}{\Delta x_i} \leq C_{max} \tag{13}$$

Where u_i is the velocity in the direction i, and Δx_i the spacing between points of discretisation used for the finite difference method. The constant C_{max} depends on the equations and the physical phenomena to solve. A physical meaning of Eq.(13), is perhaps a relation between the traveled distance during a time step and the discretisation's spacing. In fact, it seams reasonable limiting the particle displacement during a time step. This appears to be a reasonable limit on particle displacement during a time step.

A stability condition mentioned by Gerstle[9], for problems with a single degree of freedom under unforced vibration is given in Eq.(14).

$$\Delta t_{cr} \leq \frac{2}{\omega_n} \left(\sqrt{1+\xi^2} - \xi \right) \tag{14}$$

Here ω_n represents the natural vibration frequency, and ξ the damping ratio. Eq.(14) can be used for a initial estimation of Δt_{cr} , for multiple degree of freedom if a previous knowledge of the principal of the structure exists.

A second alternative condition proposed by Gerstle[9], and described in Eq.(18), is it is based on the capacity of representing a pulse of the vibration through the structure.

$$\Delta t_{cr} \leq \frac{\Delta x_i}{\pi c_0} \left(\sqrt{1+\xi^2} - \xi \right) \tag{15}$$

Where c_0 is the sound speed in the linear elastic solid, given by Eq.(19).

$$c_0 = \sqrt{\frac{K}{\rho}} \tag{16}$$

Where K is the bulk modulus and ρ is the density of the material. The bulk modulus is given by Eq.(17).

$$K = \frac{E}{3(1-2\nu)} \tag{17}$$

Where E is the elasticity modulus and ν is the Poisson's ratio of the material. If the problem is not history dependent and the analysis not focused on the transitory response, then it may happen that increasing the critical time step produce no significant changes in the final steady state. However, in the presence of damage or plastic flow history dependency of the steady solution should be considered.

8 Classical elastic properties

As stated before the interaction function describes the constitutive behaviour of the material, therefore it determines the elastic modulus and the Poissons ratio of the material. The simplest way of establishing the connection between interaction function parameters and the classical elastic properties is perhaps empirically. According to the classical theory the reaction force F developed by a simple bar subjected to a small displacement δ in the axial direction is determined according to Eq.(18).

$$\frac{F}{\delta} = \frac{EA}{L} \tag{18}$$

Where A is the cross–sectional area and L is length of the bar. The fiber's stiffness parameter K of the interaction function was related with the elastic modulus, considering Eq.(18) and the geometry of the model from Fig.2(b). Firstly, a tensile displacement $\delta = 10mm$ in the axial direction was applied and the reaction force F computed, using the particle algorithm. Secondly, the elasticity modulus E was determined employing Eq.(18).
By varying the fiber's stiffness parameter K, different values of elasticity modulus E were obtained, the obtained values are represented Fig.10.

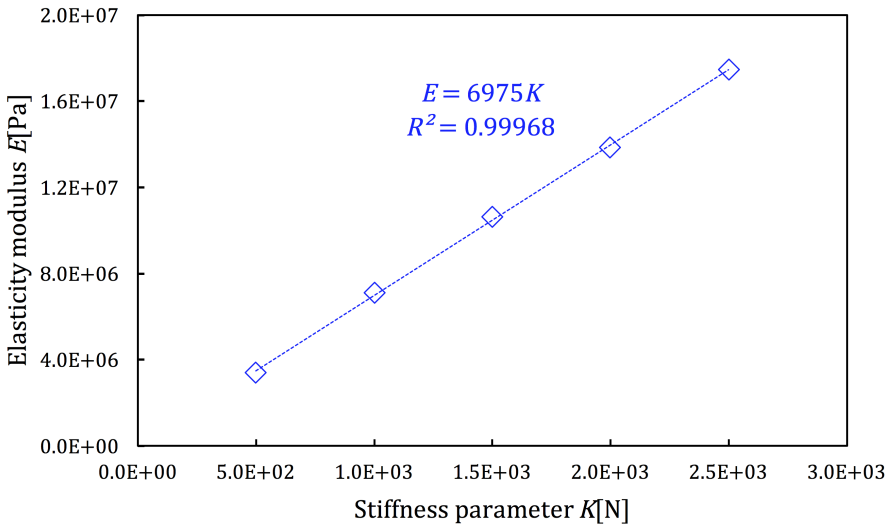

Figure 10: Relation between elasticity modulus and the stiffness parameter.

The relation obtained between the stiffness parameter and the elastic modulus is linear, therefore can be defined according to Eq.(19).

$$E = \psi_c K \tag{19}$$

Here ψ_c is a correlation parameter, with an approximate value 6975m^{-2} for this particular model. Notice that, this parameter may vary depending not only on the interaction function considered but also on the initial distribution of the particles (i.e. the lattice structure considered and the offset between particles) and the minimum interaction distance between particles.
Although this relation may be derived analytically for particular conditions, only the empirical method described above was considered, since it is relatively simple and effective.

9 Example with cracking

A simply supported beam, schematized in Fig.11, was subjected to a vertical displacement in the mid span $\delta_{max} = 20\text{mm}$.
The cross section is composed by a bulk material similar elasticity as simple concrete C16/20 and reinforced with bars of a linear elastic material. The properties of the cross section materials are indicated in Tab.5.

The beam model was discretised with 13.5 thousand particles and 2.71 million fibres connecting the particles. Fig.12 shows the damage levels obtained for at 37% of the maximum displacement. It was found that damage by spalling, develops in the region where the displacement is applied and near the supports, due to the concentrated stress, as is apparent in Fig.12 . The failure occurs in shear due to the absence of transverse reinforcement in the beam, as shown in Fig.13 .
The diagram of Fig.14, represents the evolution of the moment in the mid-span with the imposed displacement ratio δ/δ_{max}. That diagram describes an initial reduction of the resistant moment

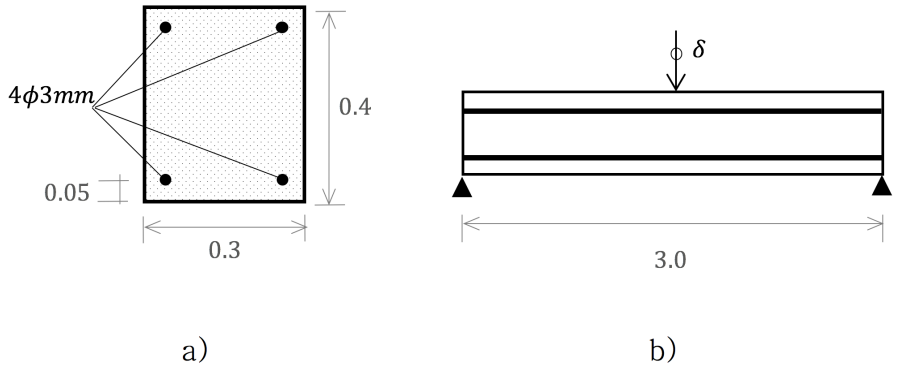

Figure 11: Geometry and boundary conditions of a simple supported beam: a) reinforced cross section; b) support conditions and solicitation (no transverse bars were used, dimensions in meters).

Table 5: Parameters of the materials.

Bulk material			Reinforcement	
E_c	ν_c	Tensile strength f_{ct}	E_s	ν_s
20GPa	0.25	2.0MPa	200GPa	0.25

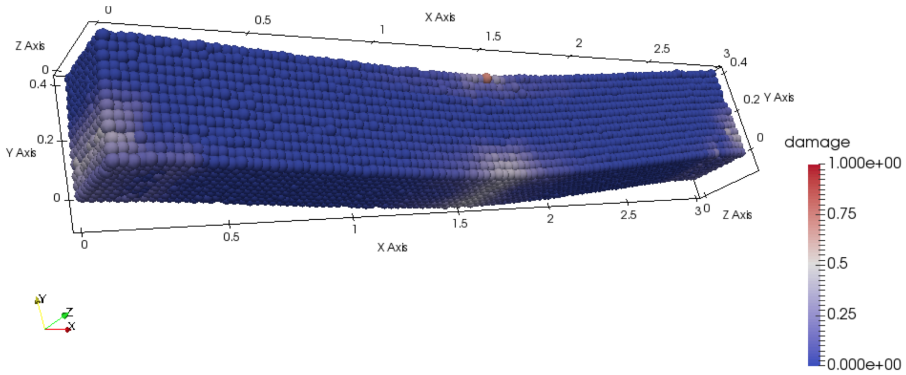

Figure 12: Damage for $\delta = 0.37\delta_{max}$ (displacements scaled 10 times).

followed by a sudden reduction of the resistant moment as the imposed displacement progresses. This sudden reduction corresponds to the brittle failure of the beam depicted in Fig.13.

10 Future work and conclusions

The described particle dynamic model, provided accurate predictions under the linear elastic regime, as it was demonstrated by the presented examples. It was verified the capability of the model of reproducing: damage mechanisms, formation of discrete cracks and reduction of load carrying capacity. As expected no numerical issues emerged directly from the disruption of continuity of the material as frequently happens when employing the finite element method. The stability of the method and a procedure to obtain equivalent elastic modulus are briefly discussed. Nevertheless, several improvements in the model should be developed in the future, namely:

- improvements in the stability of the method;

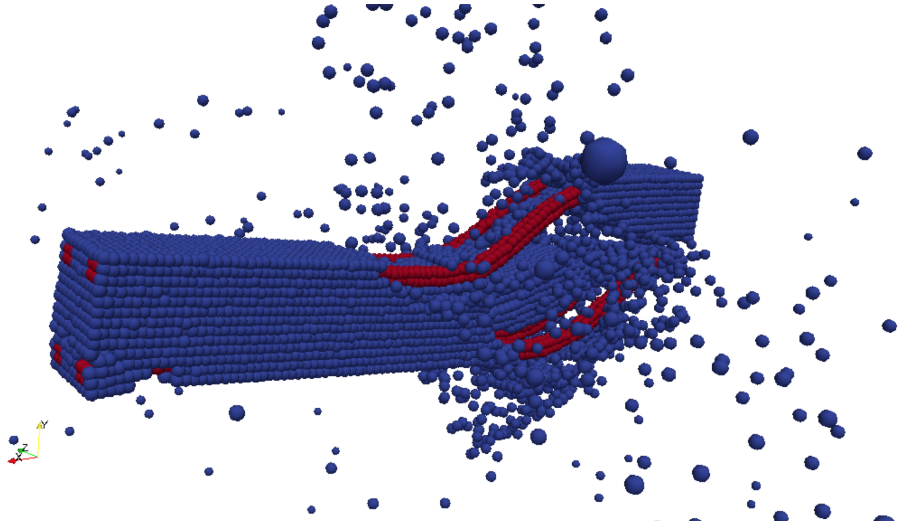

Figure 13: Deformed configuration for $\delta = 0.79\delta_{max}$ (displacements scaled 10 times, bulk material in blue and reinforcement in red).

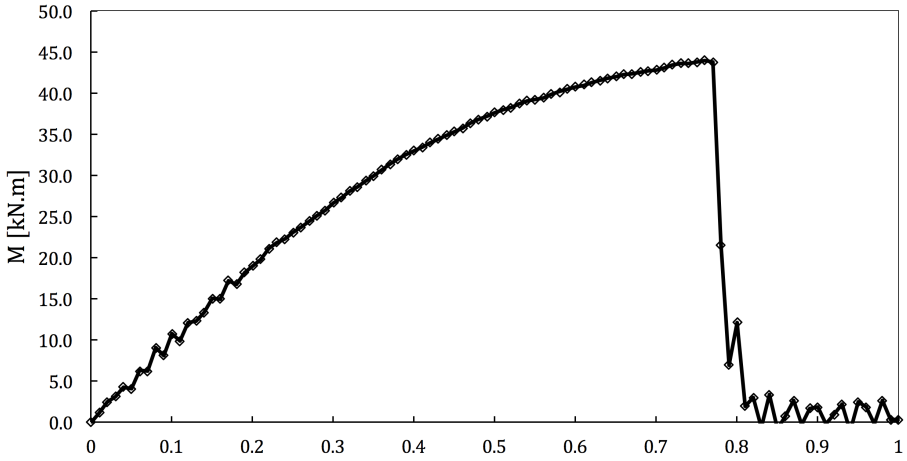

Figure 14: Evolution of the moment in the middle section with the displacement.

- sensitivity tests;
- study of different methods to generate the initial distribution of particles;
- comparison of predictions with laboratory tests.

This paper has demonstrated the quality of the proposed approach in the linear elastic regime, and its ability to reproduce disruptions in continuity whilst avoiding the usual issues that arise in the classical theory. The presented framework will be advanced in future work to improve our damage theories for materials and structures vulnerable to cracking.

Acknowledgements

This research was supported by the project, “Concrete Modelled Using Random Elements ”, EP/M020908/1.

Data access statement

All data created during this research are openly available from the University of Bath data archive at http://doi.org/10.15125/BATH-00194.

References

[1] Stewart A Silling. Reformulation of elasticity theory for discontinuities and long-range forces. *Journal of the Mechanics and Physics of Solids*, 48(1):175–209, 2000.

[2] John C. Butcher. *Numerical Methods for Ordinary Differential Equations*. Wiley & Sons, New York, 2003.

[3] Stewart A Silling, M Epton, O Weckner, J Xu, and E Askari. Peridynamic states and constitutive modeling. *Journal of Elasticity*, 88(2):151–184, 2007.

[4] Stewart A Silling and Ebrahim Askari. A meshfree method based on the peridynamic model of solid mechanics. *Computers & structures*, 83(17):1526–1535, 2005.

[5] Walter Gerstle, Nicolas Sau, and Stewart Silling. Peridynamic modeling of concrete structures. *Nuclear engineering and design*, 237(12):1250–1258, 2007.

[6] W Gerstle, N Sau, and E Aguilera. Micropolar peridynamic modeling of concrete structures. In *Proceedings of the 6th international conference on fracture mechanics of concrete structures*, 2007.

[7] H D. Miranda, C J K. Williams, and J. Orr. Peridynamics for concrete structures a new explicit analysis method. In *9th International Concrete Conference*, Dundee, Scotland, 2016.

[8] C J K Williams. Meshfree peridynamic computer modeling of concrete in three dimensions using randomly positioned particles. In *Proceedings of the Second International conference on flexible formwork*, 2012.

[9] Walter Gerstle. *Introduction to practical peridynamics: computational Solid Mechanics Without Stress and Strain*. World Scientific, 2015.

[10] Amy Henderson Squillacote and James Ahrens. *The paraview guide*, volume 366. Kitware, 2007.

[11] Desmond J Higham and Nicholas J Higham. *MATLAB guide*. Siam, 2005.

[12] Hibbett, Karlsson, Sorensen, and Hibbitt. *ABAQUS/standard: User’s Manual*, volume 1. Hibbitt, Karlsson & Sorensen, 1998.

[13] Richard Courant, Kurt Friedrichs, and Hans Lewy. On the partial difference equations of mathematical physics. *IBM journal*, 11(2):215–234, 1967.